Available online at www.sciencedirect.com

ScienceDirect

IFAC PapersOnLine 55-37 (2022) 288–294

Design of Asymmetric Parallel Manipulator for Axial-Bending Dynamic Stiffness Analysis

Andres Torres* Ahmed Soliman Guilherme Ribeiro** Nina Mahmoudian* Mo Rastgaar****

**Department of Mechanical Engineering, Purdue University, West Lafayette, IN 47906, USA (e-mail: gtorresr@purdue.edu (A.T))*

***Polytechnic Institute, Purdue University, West Lafayette, IN 47906, USA (e-mail: solimana@purdue.edu (A.S.), garamizo@mtu.edu (G.R.), rastgaar@purdue.edu (M.R.))*

Abstract: This paper presents an asymmetric 5-bar parallel manipulator capable of characterizing the dynamic stiffness properties of materials used in robotic joints in 2 degrees of freedom, axial and bending, simultaneously. The end effector is actuated by two stepper motors with linear rails. Two force sensors were added to estimate axial force and moment. Experiments were performed in axial compression, bending, and a mixed axial-bending motion. A spring-mass-spring system was constructed to evaluate the fabricated apparatus for frequency analysis up to 20Hz. The frequency analysis result was accurate when compared to the theoretical response of the system. Axial stiffness estimation had an error of 1.5%, bending stiffness had an error of 3.4%, and mixed-mode had a total error of 1.8%. Future experiments will showcase the versatility of the apparatus and test nonlinear samples.

Keywords: material characterization, frequency response, 2 degrees of freedom, dynamic mechanical analyzer, 5-bar, mechanism

1. INTRODUCTION

Successful system identification of mechanical components allows engineers to predict their dynamic responses to different inputs. There are many mechanical properties and therefore many tools to test different properties [Henriques et al. (2018)]. For example, one of the most ubiquitous pieces of equipment is the universal testing machine, which is used to test axial stress-strain relationships and identify properties like Young's modulus, yield strength, and ultimate strength [Mathew and Francis (2019); Prost et al. (2018)]. Other tools like dynamic mechanical analyzers (DMA) study viscous and elastic properties of a sample under an oscillating load and compare against temperature, time, or frequency [Greonewoud (2001)]. Impact hammers are another tool commonly used in modal tests, where a hammer, with a force transducer on the head and an accelerometer on the body, is used to strike a structure to create impulse responses rich in frequency data and ultimately determine dynamic mechanical properties [Ozdoganlar et al. (2005)]. Nevertheless, new apparatus that have the flexibility or specialization for a specific task or type of measurement are needed. For example, [HemaLatha et al. (2018)] built a bi-axial testing machine and [Ogawa et al. (2019)] built a multiaxial bending-torsion fatigue machine, both illustrating new testing methods based on the fundamentals of simpler tests.

Parallel manipulators are a type of configuration whose end-effector is attached to multiple linkages, ultimately creating a closed loop of linkages and joints. Stewart platforms are a 6 degree of freedom (DOF) parallel manipulator with universal-prismatic-spherical chains connecting the ground and the end effector [Bohigas et al. (2012)]. This type of device has found wide success in flight simulations. A variant of the previous is the planar Stewart platform, which only has two axial and one rotational DOF, all in the same plane for a total of 3-DOF. A novel application for this type of robot [Soliman and Ribeiro (2022)] is attaching it to a lower leg prosthesis and including wheels on the base of the Stewart platform to extend the horizontal workspace. Commercially successful parallel manipulators include delta 3D printers, having three coupled pairs of prismatic actuators, each with two passive revolute joints [Celi et al. (2015)]. This configuration allows for a three-dimensional position workspace that doesn't change end-effector angle.

The 4-bar mechanisms have been widely used in robotic devices [Zarkandi et al. (2011)]. They have one degree of freedom, usually accompanied by one actuator. These mechanisms do not have redundant joints, and therefore, kinematics can be designed and controlled within these limitations. Another important mechanism to consider is the 5-bar mechanism, comprised of five linkages and usually two actuators. Their joints and actuators are a combination of revolute (R) and/or prismatic (P) joints. An example is a pantograph [Campion (2005)], a parallel mechanism with five linkages and five revolute joints (RRRRR), achieving 2-DOF in a plane. Moreover, [Zarkandi et al. (2011)] studied a kinematically redundant planar PRRRRRP robotic manipulator with four actuators (actuated on PR-RP) to avoid singularities typical of a 5-bar system and extend its workspace.

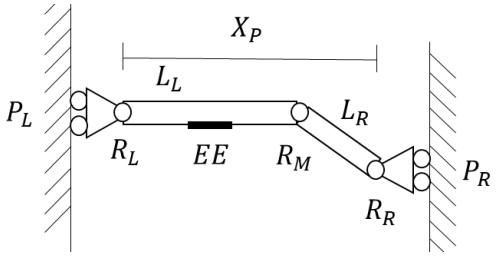

Figure 1. Kinematics diagram of proposed 5-bar mechanism

10.1016/j.ifacol.2022.11.199

The goal of this paper is to present an asymmetric 2-DOF PRRRP 5-bar system to assess dynamic characteristics of samples when the axial and bending properties are of importance. The novelty of this device is its ability to simultaneously test axial and bending properties with the flexibility of virtually changing the pivot point, test frequency (up to 20 Hz), and amplitude of the experiment. Following sections discuss the kinematic components of the apparatus, force sensing capabilities, dynamic equations, signal conditioning, and various tests showcasing the versatility of the design.

2. 5-BAR MECHANISM DESIGN

2.1 Kinematics Overview

The proposed parallel robot is primarily composed of two prismatic actuators, connected by two linkages and three revolute joints, as shown in Figure 1 and 2. The two prismatic actuators are vertical and parallel to each other. Linkage is abbreviated as *L*, revolute is *R,* and prismatic is *P*. Subscripts *L*, *R,* and *M* stand for left, right, and middle, respectively. X_R is the effective distance between prismatic joins, specifically the distance between R_L and R_R. The end effector (*EE*) is represented by the black rectangle below linkage L_L.

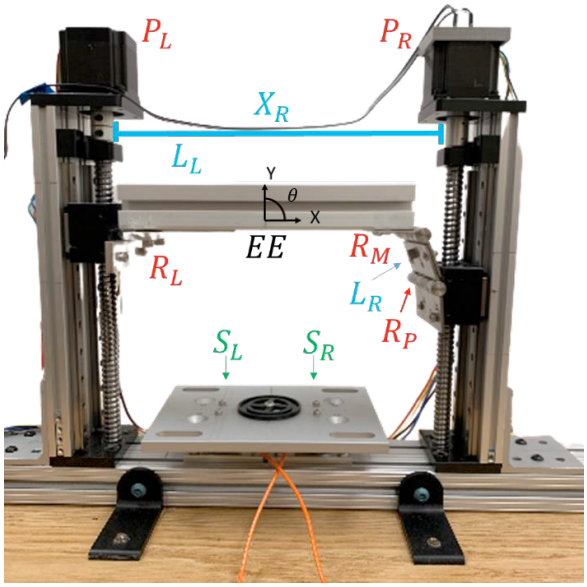

Figure 2. Assembled 5-bar Mechanism. Red symbols represent joints, blue symbols are linkages, green symbols are force sensors and the black symbol is the end effector.

Generally, 5-bar mechanisms have five linkages; however, the linkages connecting a set of prismatic joint to revolute joint is considered as having zero length. This accounts for two additional linkages. The fifth linkage is regarded as the ground; it can be thought of as the fixture connecting both prismatic joints to the benchtop. With these five linkages, we can obtain a closed chain mechanism. Kutsbach's equation is used to verify the degrees of freedom (DOF) for the planar mechanism:

$$DOF = 3(Bodies - 1) - (Constraints) \quad (1)$$

where DOF is a function of the number of bodies and the sum of constrained degrees of freedom. With five bodies and five joints, each joint constrained in two planar dimensions then:

$$DOF = 3(5 - 1) - (2 \times 5) = \mathbf{2} \quad (2)$$

2.2. Kinematic Structural Components

This section covers the components used to build the 5-bar mechanism shown in Figure 1 and 2. Prismatic actuators P_L and P_R were installed as 200mm linear rails powered by NEMA23 stepper motors (Linear Rails SFU1605 with NEMA17 Stepper Motor, Befenybay, China). Revolute joints *R* were constructed as bearing hinges. Linkage L_R is the segment between two connected hinges. Linkage L_L is an 80/20 bar. The final effective dimensions for the mechanism are L_L = 25.7 cm, L_R = 4.7 cm and X_R = 27.2 cm.

2.3. Motor Control

A Teensy 4.0 microcontroller unit (Teensy 4.0, PJRC, USA) was used as the main control unit (MCU). The control algorithm was developed in Arduino using the open source library *AccelStepper* (AccelStepper, AirSpayce Pty Ltd™). This library was chosen because it provided more customization than using the simpler *Stepper* library. Since each NEMA23 stepper motor has a 3A current requirement, which is greater than the supply of the Teensy 4.0, a TB6600 stepper motor driver was used to interface the motors, MCU and an adjustable power supply. The vertical displacement resolution of the linear actuators was calculated by:

$$Vertical\ Resolution = (Step\ Angle)(Pitch) \quad (3)$$

With a step angle of 1.8 degrees and a pitch of 5mm/rev, the linear rails have a vertical displacement resolution of 0.025 mm. This was further improved by using the motor driver's micro-stepping capabilities, preliminary testing suggested that dividing the step into eight micro-steps (0.003125mm) provided the best balance between smooth displacement and top speed.

2.4 Simulation, Jacobian and Workspace

The proposed 5-bar mechanism was recreated in MATLAB/Simulink using the measured dimensions of the mechanism. This allows us to further study the forward kinematics, inverse kinematics and the position workspace.

The Jacobian matrix [**J**] contains parameters that relate joint velocities and end effector velocity. Considering that the mechanism has two actuated prismatic joints, and two controllable states, a 2 × 2 Jacobian matrix can be constructed.

$$\begin{bmatrix} \dot{Y} \\ \dot{\theta} \end{bmatrix} = [\mathbf{J}] \begin{bmatrix} \dot{P}_L \\ \dot{P}_R \end{bmatrix} = \begin{bmatrix} J_{11} & J_{12} \\ J_{21} & J_{22} \end{bmatrix} \begin{bmatrix} \dot{P}_L \\ \dot{P}_R \end{bmatrix} \quad (4)$$

The planar coordinate $\dot{Y}$ represents the end effector's vertical velocity, and $\dot{\theta}$ as its angular velocity. Variables $\dot{P}_L$ and $\dot{P}_R$ are the left and right prismatic joint rates. For such mechanism, it is ideal if the Jacobian matrix is made up of functions that use output states to update joint velocities. However, the research team opted to use scalar values since the operational range of the end effector will have limited variation in the angular range, and thus, small angle approximation is reasonable. In this case, using scalar values for the Jacobian matrix makes it equal to the forward kinematics transformation matrix.

The Jacobian was obtained using the Simulink model. Data relating joint and end-effector velocities was obtained by moving the prismatic joints asynchronously. The maximum

end-effector angle for this data set is within ± 0.2 radians. When using small angle approximations, the maximum angle error is 0.65%.

By performing a least-squares linear regression (using MATLAB's function *fitlm*), Jacobian parameters were estimated, shown in Table 1. Furthermore, the inverse Jacobian which governs the inverse kinematics, relating the desired end effector state to the required prismatic joint actuation. Equation 5 shows the implementation of the inverse Jacobian and its calculated values.

Table 1. Jacobian Parameters

Parameter	Estimated Value	R^2
J_{11}	0.5002	0.999976
J_{12}	0.4998	
J_{21}	-0.0039020	0.999646
J_{22}	0.0039018	

$$\begin{bmatrix} \dot{P}_L \\ \dot{P}_R \end{bmatrix} = [J]^{-1} \begin{bmatrix} \dot{Y} \\ \dot{\theta} \end{bmatrix} = \begin{bmatrix} 1.000 & -128.1 \\ 1.000 & 128.1 \end{bmatrix} \begin{bmatrix} \dot{Y} \\ \dot{\theta} \end{bmatrix} \quad (5)$$

The position workspace of the proposed mechanism, presented in Figure 3, was determined by the degrees of freedom of interest; the vertical displacement Y and angle θ. Horizontal displacement is considered negligible. To identify this workspace, we first estimated the effective prismatic joint limits and conducted a simulation constrained by those parameters. Different to its symmetric counterparts [Prasad et al. (2018)], this 5-bar system has a slight asymmetric workspace due to the difference in lengths between L_L and L_R, and the position of end effector *EE*.

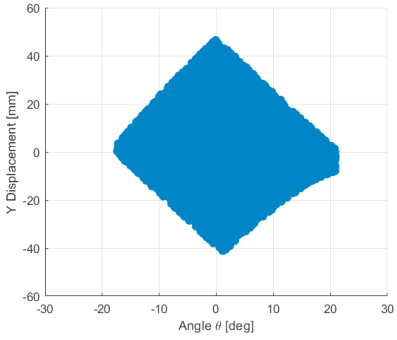

Figure 3. Y- θ workspace of asymmetric5-bar mechanism

3. MEASUREMENTS

3.1 Measurements Overview

The objective of this 5-bar mechanism is to provide the force and displacement data required for estimating the mechanical properties of a second-order system through a system identification approach. The scope of this paper covers experiments with a linear coil springs as well as a spring-mass-spring arrangement. Future applications include characterization of non-linear spring-dampers such as silicone rubber components for universal joint stiffness.

A Teensy 3.6 (Teensy 3.6, PJRC, USA) was used as the main data acquisition unit. Let's refer to this Teensy 3.6 as DAQ to differentiate it from the Teensy 4.0 (referred to as MCU) used to control the mechanism. The DAQ interfaced with Simulink at a baud rate of 1 MBd and a serial communication block sample time of 0.1s using 8bit unsigned integers. The DAQ was also connected to an AS5600 magnetic encoder (AS5600 Magnetic Encoder, UMLIFE, China) and two DYZ column type force sensors (DYZ-101 Column Type, Calt, China). Sensor sampling rate was of 1000Hz. Implementation details are discussed in the following sections. Force sensors and encoder are shown in Figure 4.

3.2 Encoder

The AS5600 magnetic encoder uses hall effect principle to determine the absolute angle of circular magnet. The magnet was attached to the right prismatic joint P_R, over the stepper motor's shaft. A custom-made 3D printed adapter was fabricated to suspend the encoder above the magnet. The resolution of this encoder is 1 degree (0.0175 radians), which results in 0.014 mm vertical displacement resolution. This encoder sent measurement data to the DAQ via an I^2C communication protocol. In MATLAB, encoder data was filtered using the *hampel* function to remove outliers.

3.3 Force Sensors and Amplifiers

Two DYZ column type force sensors were placed at the base of the mechanism, spaced 9.25 cm, and screwed down to a machined aluminum plate. Each sensor is rated to a maximum of 98 N. Thus, the maximum measurable force is 196 N, twice the rate of each sensor. Each force sensor was connected to a FUTEK load cell amplifier, model IAA100, and each load cell was connected to the DAQ. Each sensor was calibrated to a 4-point linear fit with known weights: 0 kg, 2.27 kg (5lb), 4.53 kg (10 lb) and 9.07 kg (20 lb), one sensor at a time. Voltage-force response was linear. Since all experiments were oscillatory tests, force measurements were filtered using MATLAB's *fir1* function. Filter settings were set to an order of 1000 and cut-off frequency of 10 times the experiment frequency.

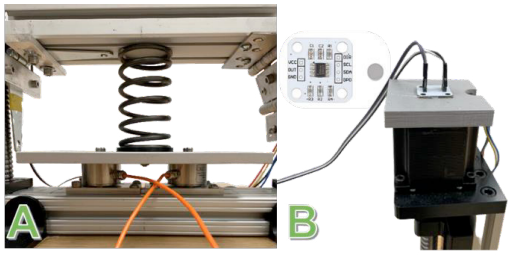

Figure 4. (A) Two axial force sensors under a horizontal aluminum plate with a test spring above. (B) Magnetic Encoder attached to stepper motor P_R. Grey 3D printed piece spaces magnet and sensor.

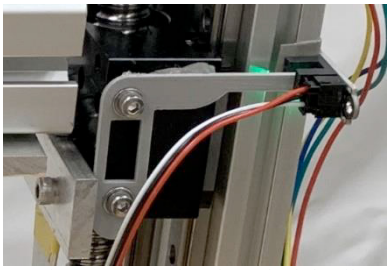

Figure 5. Optical Endstop for left rail

3.4 Axis Endstops

Optical endstops (Optical Endstop, MakerHawk, China) were implemented on each prismatic joint, as shown in Figure 5. Optical endstops were chosen because they are more robust and accurate than switch endstops and simpler to implement than hall-effect endstops. A 3D printed L shape piece was attached to each prismatic joint to interrupt the light emitter at the endstop. A home-reset protocol was developed on Arduino, so that every time an experiment was performed, the manipulator resets the end effector position to a known height and zero angle before conducting the test. The optical end stops were connected to the MCU.

4. TEST PROTOCOLS

Multiple tests were conducted to showcase the versatility of this device. In addition, a validation experiment was conducted to assess the accuracy of the measurements. This section discusses the protocols followed for each test method, experiment parameters and the experimental results.

4.1 Validation Experiment for Axial Compression & Bending

The stiffness of a metal coil spring was measured using a 6-DOF force plate (Type 9260AA, Kistler, Switzerland) and an infrared motion capture system (Miqus, Qualysis, Sweden). The spring was attached to an aluminum plate with reflective markers, as shown in Figure 6. In the Qualysis software, the top five markers produce a rigid body. By using the vertical displacement data from the rigid body and the force data from the force plate, a least-squares linear regression was performed using equation 8 to find the stiffness of the spring, as shown in Figure 7. The stiffness was determined to be 11.16 N/mm. This value will be used to assess the axial testing capabilities of the parallel manipulator.

Figure 6. Validation test set up. Linear test spring has aluminum plate on top with markers. Blue force plate measures force reactions.

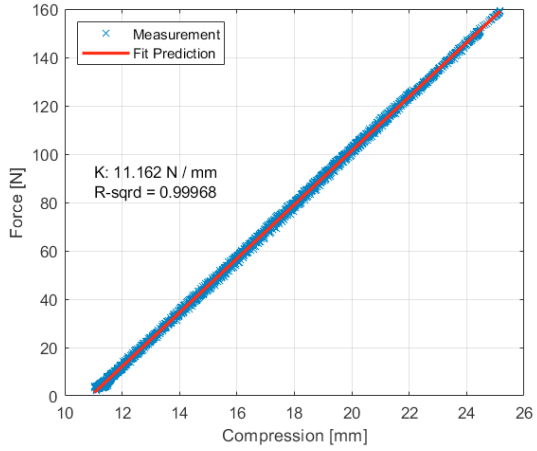

Figure 7. Validation test results for coil spring under axial compression.

Another test was performed to find the bending stiffness of the spring. Using the same set up as the axial test, the spring top was pivoted back and forth, and bending moment was measured by the force plate. Figure 8 shows the data and linear fit for the moment versus rotation plot. Bending stiffness, was estimated to 13.2 Nm/rad.

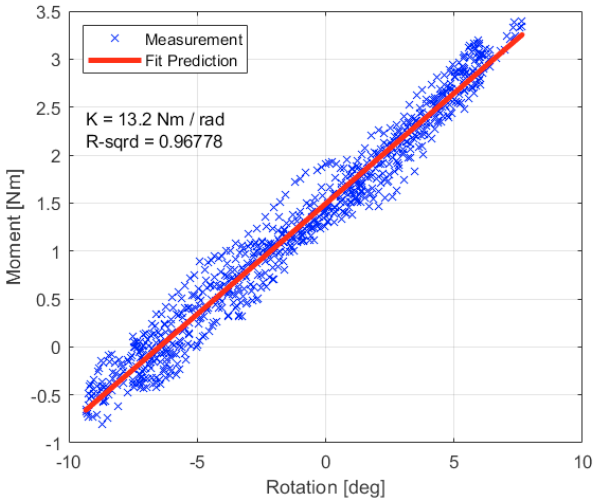

Figure 8. Validation test results for coil spring under bending.

4.2 Axial compression test

The schematic of the linear axial spring is shown in Figure 9. By slowly oscillating the end effector in the vertical Y axis, the reaction forces measured by both sensors are equal, as they are equidistant from the spring. The total force acting on the spring, F, is given by equation 6.

$$F = S_1 + S_2 \tag{6}$$

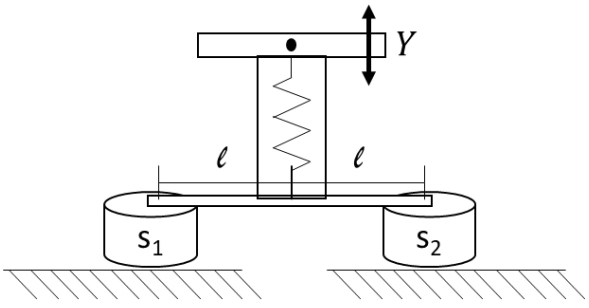

Figure 9. Axial spring compression test

Where S_1 and S_2 are the forces measured by the left and right sensors, respectively.

4.3 Pure Bending of a Spring

Pure bending motion can be achieved by rotating the end effector, as shown in Figure 10. Any bending motion on the top of the spring will cause a moment reaction on the bottom. Thus, we can analyze the relationship for moment and rotation to find rotational stiffness of a spring. The moment on the spring can be calculated by the individual forces of each sensor and their relative distance, as shown in equation 7.

$$\tau = l(\Delta S_1 - \Delta S_2) \quad (7)$$

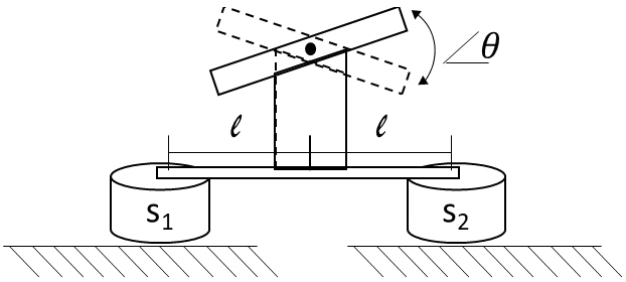

Figure 10. Rotational spring test

4.4 Mixed Mode: Axial Compression and Bending

Mixed axial compression and bending can be achieved by moving the prismatic actuators at different speeds, thus the end-effector would move in the vertical and rotational axis (Figure 11). It is possible to create infinitely many combinations of axial and bending inputs by varying the amplitude, frequency and phase of each state. This paper presents one possibility of mixed-mode compression by only actuating the right prismatic actuator. Effectively, this lever arm has a length equal to half the span of linkage L_L. A controller was created to modify the virtual pivot point on any point along the axis of the horizontal end-effector bar.

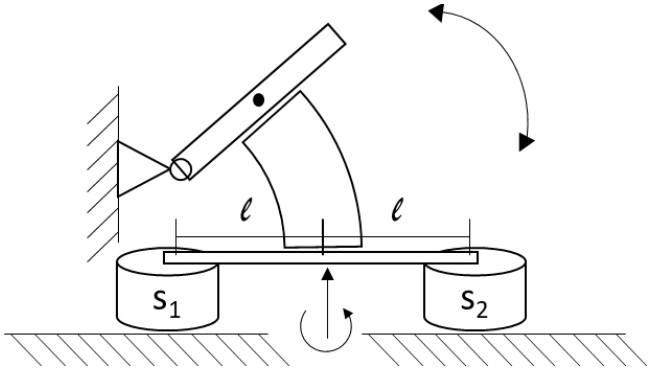

Figure 11. Mixed axial compression and bending test

All stiffnesses were estimated considering the relationship between displacement and force:

$$K_X = \frac{\Delta F}{\Delta X} = \frac{\Delta S_1 + \Delta S_2}{\Delta X} \quad (8)$$

$$K_\theta = \frac{\Delta \tau}{\Delta \theta} = \frac{l(\Delta S_1 - \Delta S_2)}{\Delta \theta} \quad (9)$$

$$\begin{bmatrix} \Delta F \\ \Delta \tau \end{bmatrix} = \begin{bmatrix} K_X & K_{X\theta} \\ K_{\theta X} & K_\theta \end{bmatrix} \begin{bmatrix} \Delta X \\ \Delta \theta \end{bmatrix} \quad (10)$$

where K_X is the axial stiffness and K_θ is the rotational stiffness. Equation 10 considers the effect of dynamically coupled properties, including $K_{X\theta}$, the axial stiffness provided by bending and $K_{\theta X}$, the rotational stiffness provided axial compression. These coupled properties were not computed because the systems tested did not have any intrinsic coupled properties we could validate and also the test performed has the same frequency and phase for X and θ, meaning that coupled dynamics would be unobservable in that experiment.

4.5 Axial Frequency Response of Spring-Mass-Spring

In order to test the ability of the proposed parallel manipulator for dynamic testing, a frequency test was developed. The test consists of using a spring-mass-spring system with predictable frequency response. The spring-mass-spring system, shown in Figure 12, has three main components, spring #1, a mass, and spring #2, represented by parameters K_1, M, and K_2, respectively.

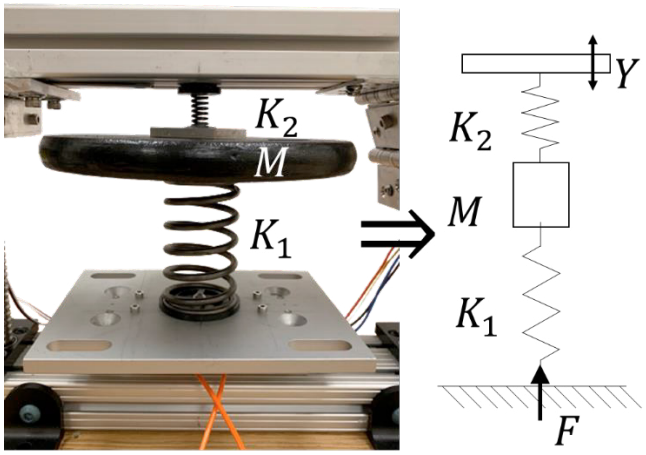

Figure 12. Spring-mas-spring system for dynamic test, with attachments.

The analytical transfer function for the system in Figure 12 was determined to be:

$$\frac{F(s)}{Y(s)} = \frac{-K_1 K_2}{Ms^2 + Bs + (K_1 + K_2)} \quad (11)$$

where B is the viscous damping. We can approximate B, assuming it is a small value, to avoid a large amplitude at the resonance frequency. For this experiment, we will select B to match the magnitude of the resonance. The parameters used were the following: $K_1 = 11162 \frac{N}{m}$, $K_2 = 10780 \frac{N}{m}$, $B \approx 15 \frac{N\,s}{m}$, and $M = 4.6\,kg$. The resulting frequency response is included in figures 17 and 18, along with the experimental results.

5. EXPERIMENT PARAMETERS & RESULTS

The axial compression test was performed at a frequency of 0.1 Hz and amplitude of 1 mm. Results are shown in Figure 13. Stiffness estimation (K_X = 10.99 N/mm) is very similar to the independent validation test using the motion capture system and force plate (K_X = 11.16 N/mm). The relative error of the axial test to the validation test is 1.5%. This error may be attributed to compounding error sources across devices. There seemed to be a force measurement disturbance when both motors changed velocity direction at the peaks of oscillation, which was reduced by the low pass filter. More studies will be conducted to identify and reduce error sources.

The pure bending experiment was performed at 0.1 Hz and an amplitude of 5 degrees. Results are shown in Figure 14. Overall the fitting went well, with a bending stiffness of K_θ = 13.65 Nm/rad. Compared to the validation bending stiffness (K_θ = 13.20 Nm/rad), the relative error of the bending stiffness estimation is 3.4%. There seems to be a slight curving of the trajectory. This may be due to using a Jacobian matrix with

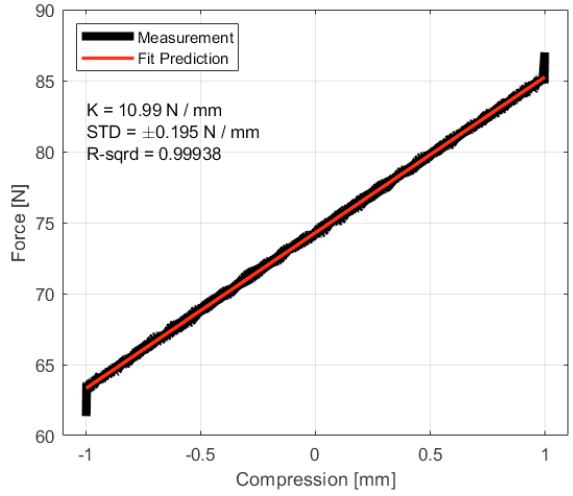

Figure 13. Axial compression result

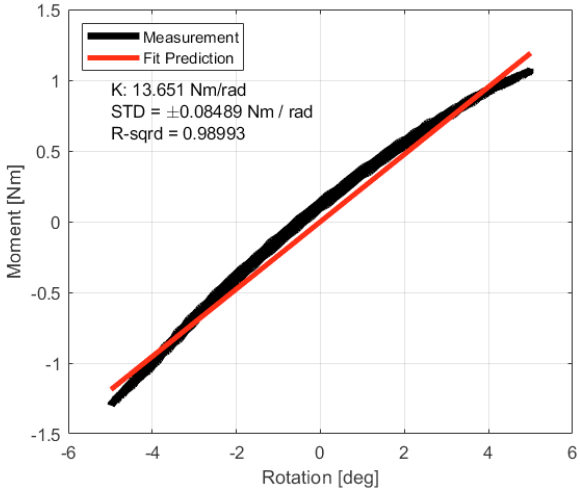

Figure 14. Bending test, moment-angle plot

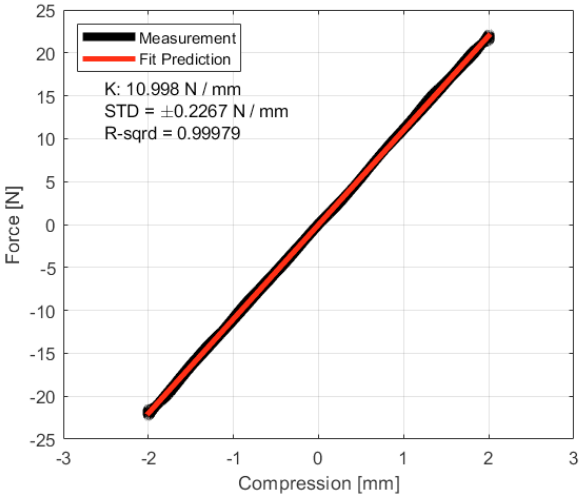

Figure 15. Axial component of mixed mode analysis

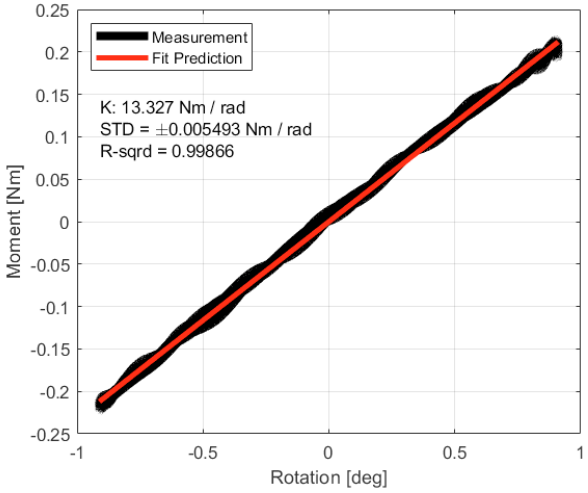

Figure 16. Bending component of mixed mode analysis

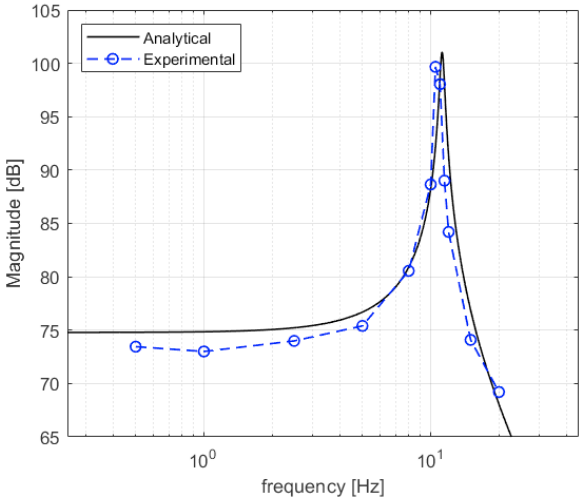

Figure 17. Magnitude plot of frequency analysis. Analytical solution is solid black line. Blue markers represent experimental data points.

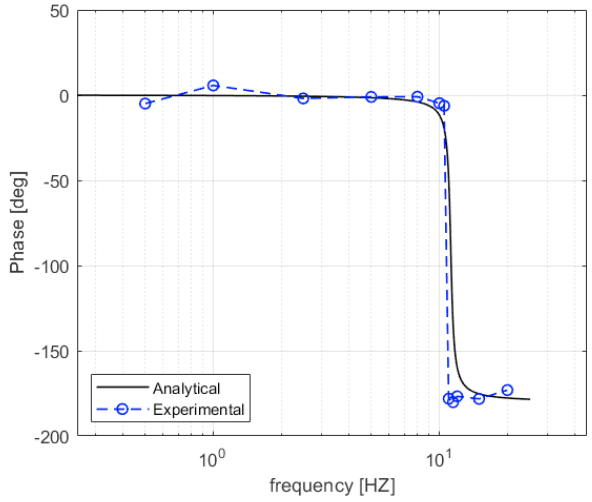

Figure 18. Phase plot of frequency analysis. Analytical solution is solid black line. Blue markers represent experimental data points.

fixed rates at large amplitudes or because the spring has a spiral shape with grounded ends.

The mixed axial-bending experiment was separated into its two components, presented in figures 15 and 16. Oscillation frequency was 0.1 Hz and lever arm was 0.125 m. Both stiffnesses are similar to the single degree experiments. Axial stiffness was virtually the same to the axial compression test, meaning that the error was still 1.5%. Bending stiffness was estimated to be K_θ = 13.327 Nm/rad. The relative error to the validation bending stiffness is of 0.96%. Thus, the total relative error (root mean squared) is 1.8%. This result outperforms the bending-only test. This inconsistency is an area of improvement that will be addressed in the future. Still, the mixed-mode test is successful and can be used in the future to analyze samples with nonlinear stiffness contributions.

The magnitude and phase frequency response plots are presented in figures 17 and 18, respectively. Oscillation amplitude was 0.2 mm. This amplitude was selected because the resonance magnitude was very high and springs were compressing to their maximum range at higher amplitudes. Experimental frequency response is similar in magnitude and phase to the analytical response. The low-frequency magnitude is slightly lower than anticipated. This may be caused by the bonding agent used to interface the springs, the weight, and the 3D printed parts used to keep the springs in place. Nevertheless, this shows the ability of the proposed 5-bar robot to perform frequency analysis up to a range of 20Hz across different response magnitudes and phases.

6. CONCLUSIONS

A 5-bar apparatus was developed to estimate mechanical properties of samples in 2 degrees of freedom; in axial and rotational directions. A compression spring was tested in two independent experiments to evaluate the accuracy of the proposed device. Other experiments such as a mixed-mode compression and frequency analysis were performed to showcase the capabilities of the device. The experiments showed that the apparatus is capable of estimating the stiffness in axial mode with 1.5% error, and in bending mode with 3.4% error, the total error in mixed mode was 1.8% error. This showed the feasibility of measuring stiffness parameters using the proposed design. Future studies should identify the overall stiffness of the 5-bar mechanism and practice stiffness estimation performance on springs stiffer than 11.16 N/mm. Nevertheless, the system is reasonably accurate for the tested stiffnesses and lower ones.

There are other areas for improvement in the future work. For instance, the magnetic encoder works well enough and it is easy to install on the motor, but a quadrature encoder may provide better resolution and would be less susceptible to electromagnetic interference. Although it is helpful to study single frequency response, as it is convenient to characterize samples with nonlinear stiffness that have properties coupled to oscillation amplitude, random input perturbations should also be used for system identification as it covers a wide range of frequency components in a single test.

References

Bohigas, Oriol & Manubens, Montserrat & Ros, Lluís. (2012). A Linear Relaxation Method for Computing Workspace Slices of the Stewart Platform. Journal of Mechanisms and Robotics. 5.

Campion, G., Qi Wang, & Hayward, V. (2005). The Pantograph Mk-II: A haptic instrument. 2005 IEEE/RSJ International Conference on Intelligent Robots and Systems.

Celi, R., Sempértegui, A., Morocho, D., Loza, D., Alulema, D., & Proaño, M. (2015). Study, design and construction of a 3D printer implemented through a delta robot. 2015 CHILEAN Conference on Electrical, Electronics Engineering, Information and Communication Technologies (CHILECON), 717–722.

Greonewoud, W. M. (2001). Dynamic Mechanical Analysis. Characterisation of Polymers by Thermal Analysis, 94–122.

HemaLatha, O., Akbar, F. M., Khan, K. A., & Minhaj, S. A. (2018). Design of bi-axial testing machine. 5(12), 9.

Henriques, I. R., Borges, L. A., Costa, M. F., Soares, B. G., & Castello, D. A. (2018). Comparisons of complex modulus provided by different DMA. Polymer Testing, 72, 394–406.

Mathew, S. J., & Francis, V. (2019). Development, Validation and Implementation of Universal Testing Machine. 69.

Ogawa, F., Shimizu, Y., Bressan, S., Morishita, T., & Itoh, T. (2019). Bending and Torsion Fatigue-Testing Machine Developed for Multiaxial Non-Proportional Loading. Metals, 9(10), 1115.

Ozdoganlar, O. B., Hansche, B. D., & Carne, T. G. (2005). Experimental modal analysis for microelectromechanical systems. Experimental Mechanics, 45(6), 498–506

Prasad, R. B., & Arif, M. (2018). Workspace and Singularity Analysis of Five Bar Planar Parallel Manipulator. *2018 5th IEEE Uttar Pradesh Section International Conference on Electrical, Electronics and Computer Engineering (UPCON)*, 1–6.

Prost, V., Olesnavage, K. M., Brett Johnson, W., Major, M. J., & Winter, A. G. (2018). Design and Testing of a Prosthetic Foot With Interchangeable Custom Springs for Evaluating Lower Leg Trajectory Error, an Optimization Metric for Prosthetic Feet. Journal of Mechanisms and Robotics, 10(2), 021010.

Soliman, A., & Ribeiro, G. A. (2022). Feasibility Design and Control of a Lower Leg Gait Emulator utilizing a Mobile 3-RPR Parallel Manipulator. 18.

Zarkandi, S., Vafadar, A., & Esmaili, M. R. (2011). PRRRRRP redundant planar parallel manipulator: Kinematics, workspace and singularity analysis. 2011 IEEE 5th International Conference on Robotics, Automation and Mechatronics (RAM), 61–66.